PNAS RESEARCH ARTICLE | NEUROSCIENCE

Dark continuous noise from mutant G90D-rhodopsin predominantly underlies congenital stationary night blindness

Zuying Chai[a,1,2], Yaqing Ye[a,1], Daniel Silverman[a,b,3], Kasey Rose[c], Alana Madura[c], Randall R. Reed[d], Jeannie Chen[c], and King-Wai Yau[a,2]

Contributed by King-Wai Yau; received March 6, 2024; accepted April 17, 2024; reviewed by Ching-Kang J. Chen and Theodore G. Wensel

Congenital stationary night blindness (CSNB) is an inherited retinal disease that causes a profound loss of rod sensitivity without severe retinal degeneration. One well-studied rhodopsin point mutant, G90D-Rho, is thought to cause CSNB because of its constitutive activity in darkness causing rod desensitization. However, the nature of this constitutive activity and its precise molecular source have not been resolved for almost 30 y. In this study, we made a knock-in (KI) mouse line with a very low expression of G90D-Rho (equal in amount to ~0.1% of normal rhodopsin, WT-Rho, in WT rods), with the remaining WT-Rho replaced by REY-Rho, a mutant with a very low efficiency of activating transducin due to a charge reversal of the highly conserved ERY motif to REY. We observed two kinds of constitutive noise: one being spontaneous isomerization (R*) of G90D-Rho at a molecular rate (R* s^{-1}) 175-fold higher than WT-Rho and the other being G90D-Rho-generated dark continuous noise comprising low-amplitude unitary events occurring at a very high molecular rate equivalent in effect to ~40,000-fold of R* s^{-1} from WT-Rho. Neither noise type originated from G90D-Opsin because exogenous 11-*cis*-retinal had no effect. Extrapolating the above observations at low (0.1%) expression of G90D-Rho to normal disease exhibited by a KI mouse model with $Rho^{G90D/WT}$ and $Rho^{G90D/G90D}$ genotypes predicts the disease condition very well quantitatively. Overall, the continuous noise from G90D-Rho therefore predominates, constituting the major equivalent background light causing rod desensitization in CSNB.

congenital stationary night blindness (CSNB) | G90D-rhodopsin | spontaneous (thermal) isomerization | dark continuous noise | background adaptation

Significance

Congenital stationary night blindness is an inherited and nonprogressive visual disorder that specifically disables rod signaling. The current speculation in the field after years of study of the mutant rhodopsin, G90D-Rho, causing disease is that this mutant holo-pigment constitutively generates a noise signal that adapts the rod sufficiently strongly to render it insensitive to scotopic light. In this work, we report success in expressing the mutant rhodopsin at a low enough level to resolve these noise events, which consist of a combination of higher-than-normal spontaneous-isomerization events and, much more importantly, overwhelmingly abundant smaller noise events composed of electrical events triggered by single active rod-transducin (G_{T1}α*)/cGMP-phosphodiesterase (PDE) complexes (G_{T1}α*·PDE*).

Rhodopsin is the photopigment found in the outer segment of rod photoreceptors, and it underlies scotopic vision. Over 150 different mutations in rhodopsin have been identified in human patients causing either retinitis pigmentosa (RP) or congenital stationary night blindness (CSNB) (1, 2). Unlike retinitis pigmentosa, which leads to progressive retinal degeneration and eventually blindness, CSNB causes a profound but stable loss of rod sensitivity without showing severe retinal degeneration (3, 4). To date, four rhodopsin mutations (G90D, T94I, A292E, and A295V) have been identified to cause CSNB, all of which affect amino acid residues near the covalent linkage between the opsin protein and its chromophore, 11-*cis*-retinal (5–7). Previous studies have indicated that dark constitutive activity from these mutations underlies the loss of rod sensitivity in CSNB patients (8–12), but the nature of the constitutive activity remains controversial.

Among the four mutations, G90D-Rho has been studied the most extensively. In WT-Rho, the salt bridge formed between E113 and K296 (which is covalently linked to the chromophore) is a key constraint maintaining the inactive state of rhodopsin both in darkness (with bound chromophore) and after light exposure (the apoprotein state without bound chromophore) (13). The negatively charged aspartate in the G90D mutant is thought to perturb this salt bridge, thus conferring to dark G90D-Rho conformational properties that are capable of activating transducin (14–16). In addition, early biochemical studies have shown that G90D-Opsin (i.e., mutant pigment protein in the absence of chromophore) exhibits much higher constitutive activity than WT-Opsin (10, 14). An electrophysiological study on transgenic *Xenopus laevis* rods expressing G90D-Rho also showed a reduction in light sensitivity and that exogenous chromophore was able to fully rescue this loss in sensitivity (11). Thus, together, these studies would suggest that the G90D-opsin activity led to the desensitization of rods in CSNB. On the other hand, these *Xenopus* results are inconsistent with the observation from G90D-human patients that this desensitization cannot be resensitized even after 12 h of dark adaptation (8), during which time the regeneration of G90D-Rho by 11-*cis*-retinal should have reached completion. This lack of resensitization by exogenous 11-*cis*-retinal was confirmed in transgenic mouse rods expressing mouse G90D-Rho, arguing against the apo-opsin hypothesis (12). Instead, it has been speculated that G90D-Rho constitutively gives rise

Author contributions: Z.C., Y.Y., D.S., R.R.R., and K.-W.Y. designed research; Z.C., Y.Y., K.R., A.M., and J.C. performed research; Z.C., Y.Y., D.S., K.R., A.M., and J.C. analyzed data; K.-W.Y. fundings; and Z.C., J.C., and K.-W.Y. wrote the paper.

Reviewers: C.-K.J.C., University of Texas Health Science Center San Antonio; and T.G.W., Baylor College of Medicine.

The authors declare no competing interest.

[1]Z.C. and Y.Y. contributed equally to this work.

[2]To whom correspondence may be addressed. Email: zchai1@jhmi.edu or kwyau@jhmi.edu.

[3]Present address: Department of Neuroscience, University of California Berkeley, Berkeley, CA 94305.

This article contains supporting information online at https://www.pnas.org/lookup/suppl/doi:10.1073/pnas.2404763121/-/DCSupplemental.

Published May 14, 2024.

to an unknown conformational state that would activate the transduction cascade with low gain, triggering unresolvable unitary activity (12).

Because the previous observations from transgenic G90D-Rho *Xenopus* (11) were inconsistent with the phenotype found in human patients (8) and also unlike that shown in transgenic mouse (12), we have decided to forego the former *Xenopus* results and its associated observations by focusing on the mouse. We generated a knock-in (KI) mouse line harboring the G90D-Rho mutant by employing the CRISPR/Cas9 technology. In designing this mouse line, we were also able to overcome one major difficulty by expressing G90D at a very low level. Up to now, the G90D-Rho disease phenotype in mouse rods has been studied in transgenic host rods containing either one (Rho^{G90D+};$Rho^{WT/-}$, ~20% G90D-Rho expression at 18-wk-old animals) or both copies ($Rho^{G90D+/+}$;$Rho^{-/-}$, ~30% G90D-Rho expression at 27-wk-old animals) of the G90D-Rho transgene (9, 12). As a result, the intrinsically high constitutive activity of G90D-Rho rendered the steady dark current substantially reduced and at the same time made the host cells heavily light-adapted due to "equivalent-background-light adaptation" (12). In the present study, we generated the KI mouse line with a deliberately very low expression level of G90D-Rho protein (comprising only ~0.1% of normal rhodopsin content) to drastically reduce the adaptation state of the host cells. As such, we were able to detect and resolve distinct types of constitutive activities from G90D-Rho in a condition as if little or no equivalent background light were present. We identified two kinds of constitutive activities from G90D-Rho. The first was a G90D-Rho-triggered spontaneous (thermal) isomerization activity higher than normal. Far more importantly, however, the second type of noise was a G90D-Rho-produced "continuous noise" in darkness comprising unitary events of smaller amplitude and at high frequency. By extrapolation from the low expression of G90D-Rho to the level of G90D-Rho expressed in diseased rods as experienced genetically by humans, we concluded that it is this second type of noise that leads to the major rod-sensitivity loss in CSNB, by triggering a large reduction in dark current as real light would and consequently a very high level of "equivalent-background-light" adaptation.

Results

Generation of a KI Mouse Line with a Very Low Expression Level of G90D-Rho. Our strategy is to produce a mouse line that expresses a low enough level of mutant G90D-Rho so that its rogue behavior can be observed and analyzed within the range of linear behavior, i.e., without driving the host rods to a highly adapted state that precludes linear analysis. Accordingly, we generated a KI mouse line by inserting the mouse G90D-Rho cDNA right before the start codon of *Arrestin-1* (*Arr1*) (mouse rod arrestin) gene, based on the finding that the mRNA level of *Arrestin-1* is ~10-fold lower than that of *WT-Rho* (17) (Fig. 1*A*). The *Arrestin-1* gene was chosen as the KI target instead of the rod transducin (*Gnat1*) gene in order to avoid interfering with $G_{T1}\alpha$'s expression level and possibly phototransduction signaling (18). Also, the heterozygous $Arr1^{+/-}$ genotype appears to have little effect on the flash response, i.e., it resembles the normal case of homozygous $Arr1^{+/+}$ (19). The $Arr1^{+/G90D}$ KI mouse line was crossed with $Rho^{REY/REY}$;$Gcaps^{-/-}$ mice. The $Rho^{REY/REY}$ genetic background was used because we have shown previously that this charge reversal from the highly conserved ERY motif to REY reduced the light sensitivity by ~7,400-fold while also maintaining the normal structure of rod outer segments (20, 21). Having a largely silent REY-Rho in place of WT-Rho allows G90D-Rho responses to be isolated and quantified. The $Gcaps^{-/-}$ background serves to increase the signal-to-noise ratio by removing the Ca^{2+}-dependent negative feedback via guanylate cyclase (22).

The action spectrum of the final genotype, $Arr1^{+/G90D}$;$Rho^{REY/REY}$;$Gcaps^{-/-}$ rods measured with dim flashes had a λ_{max} at ~490 nm (similar to that of G90D-Rho; see ref. 9), versus ~500 nm for $Arr1^{+/-}$;$Rho^{REY/REY}$;$Gcaps^{-/-}$ rods (similar to that of $Rho^{REY/REY}$;$Gcaps^{-/-}$ rods; see ref. 20) (Fig. 1*B*). Based on flash families at 500 nm, $Arr1^{+/G90D}$;$Rho^{REY/REY}$;$Gcaps^{-/-}$ rods were ~four-fold as sensitive to light compared to control $Arr1^{+/-}$;$Rho^{REY/REY}$;$Gcaps^{-/-}$ rods, so that, at dim flashes giving <5,000 photons μm^{-2} (500 nm), the response was elicited predominantly from G90D-Rho (Fig. 1 *C* and *D*). As such, from Poisson analysis of 50 to 100 dim-flash responses at 500 nm on $Arr1^{+/G90D}$;$Rho^{REY/REY}$;$Gcaps^{-/-}$ and $Arr1^{+/-}$;$Rho^{REY/REY}$;$Gcaps^{-/-}$ rods, respectively, we obtained a single-photon response of 2.8 ± 0.9 pA for G90D-Rho and 0.17 ± 0.06 pA for REY-Rho (Fig. 1 *E* and *F* and Table 1; see legend for n values). For comparison, we previously obtained 2.9 ± 1.5 pA from WT-Rho in $Rho^{WT/WT}$;$Gcaps^{-/-}$ background (21). The normal size and shape of single-photon responses in $Arr1^{+/G90D}$;$Rho^{REY/REY}$;$Gcaps^{-/-}$ rods suggested that G90D-Rho went through the same phototransduction pathway as WT-Rho after isomerization, consistent with previous biochemical studies (10, 14). From the probability of failure obtained from 50 to 100 dim responses, we calculated that the amount of G90D-Rho expressed in $Arr1^{+/G90D}$;$Rho^{REY/REY}$;$Gcaps^{-/-}$ rods was ~0.1% of normal rhodopsin content in $Rho^{WT/WT}$;$Gcaps^{-/-}$ rods based on the Poisson distribution of photon absorption (*SI Appendix, Materials and Methods*). This level of G90D-Rho turned out to be appropriate for our experiments in this work.

Dark Spontaneous Isomerization Activity of G90D-Rho in $Arr1^{+/G90D}$;$Rho^{REY/REY}$;$Gcaps^{-/-}$ rods. Recording in darkness, we observed electrical events that appeared to originate from spontaneous-isomerization (R*) activity from $Arr1^{+/G90D}$;$Rho^{REY/REY}$;$Gcaps^{-/-}$ rods (Fig. 2 *A*, *Left*). As expected, $Arr1^{+/-}$;$Rho^{REY/REY}$;$Gcaps^{-/-}$ rods did not show any visible R* events because of the small REY-Rho single-photon responses (Fig. 2 *A*, *Right*). We recorded altogether from 30 $Arr1^{+/G90D}$;$Rho^{REY/REY}$;$Gcaps^{-/-}$ rods for a total time of 300 min, and observed 25 R* events, with a probability of occurrence obeying Poisson statistics (Fig. 2*B* and legend). Thus, our measurements gave an average spontaneous-isomerization event rate of 25 R*/(300 × 60 s) per cell = 0.0014 R* s^{-1} $cell^{-1}$, for the condition of ~0.1% of G90D-Rho expression (see the previous section).

If G90D-Rho expression were at 100% of WT-Rho as in WT rods, the spontaneous isomerization rate would be 0.0014 R* s^{-1} $cell^{-1}$ × (100/0.1) = 1.4 R* s^{-1} $cell^{-1}$, which is 175-fold as high as the WT-Rho rate (0.008 ± 0.004 R* s^{-1} $cell^{-1}$; ref. 21). Despite this close to 200-fold increase in molecular rate, the rate in absolute terms caused by disease is nonetheless still quite low and insignificant, because the WT rate is very low to begin with. Thus, based on the mouse Weber–Fechner relation between rod sensitivity and background light in WT rods (Fig. 2*C*), an equivalent background light of ~1.4 R* s^{-1} would reduce rod sensitivity by only ~5%. In other words, spontaneous isomerization events from G90D-Rho alone should produce a minimal reduction in rod sensitivity.

Dark Continuous Noise from G90D-Rho. Besides spontaneous-isomerization noise, close examination of electrical recordings from $Arr1^{+/G90D}$;$Rho^{REY/REY}$;$Gcaps^{-/-}$ rods indicated that this mutant pigment produced, additionally, continuous noise in darkness consisting of concatenated electrical events of low amplitude and high frequency (Fig. 3 *A*, *Left Top*). The variance of this continuous noise in $Arr1^{+/G90D}$;$Rho^{REY/REY}$;$Gcaps^{-/-}$ rods

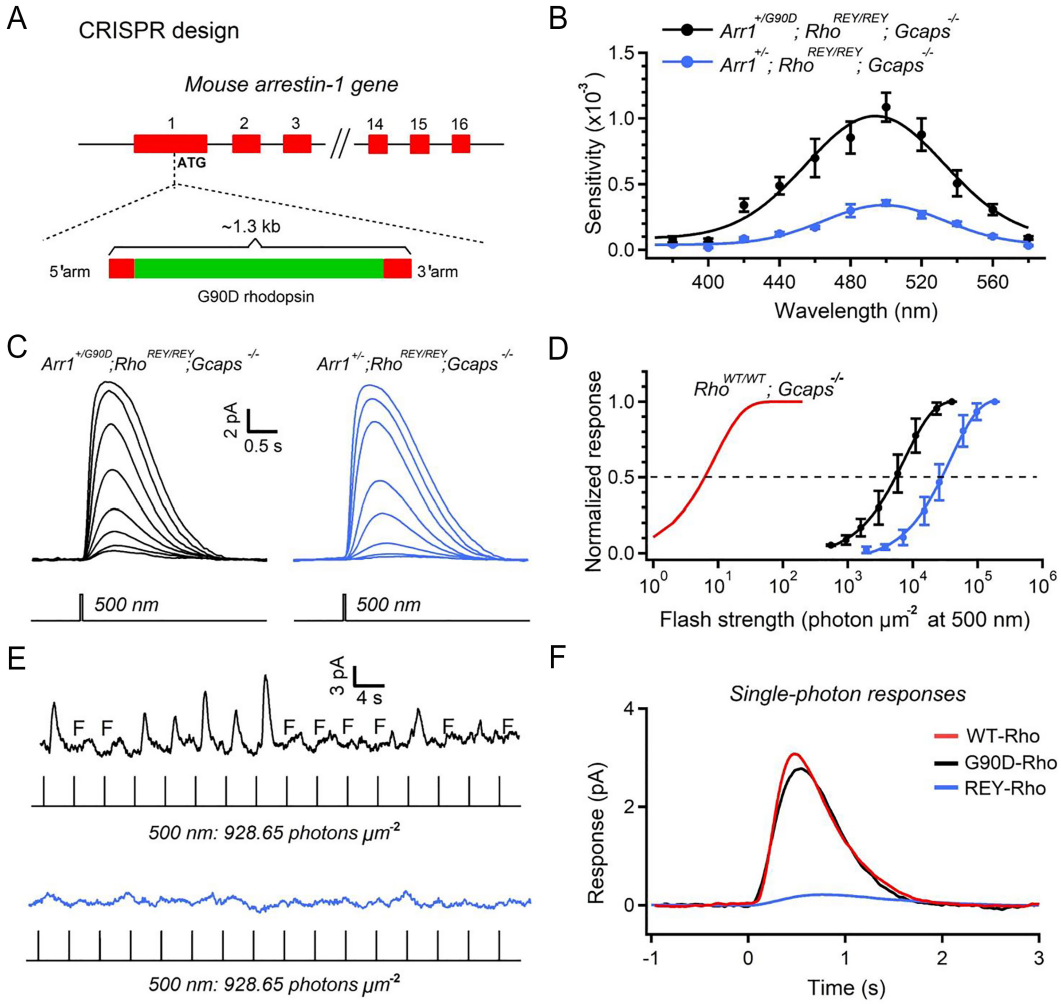

Fig. 1. Generation of a KI mouse line with low expression level of G90D-Rho. (*A*) A diagram showing the CRISPR design for making the G90D-Rho KI mouse line. A ~1.3 kb DNA fragment containing G90D-Rho cDNA was inserted before the start codon of *arrestin-1*, thus replacing the *arrestin-1* allele. (*B*) Action spectra of *Arr1*$^{+/G90D}$;*Rho*$^{REY/REY}$;*Gcaps*$^{-/-}$ (black) and *Arr1*$^{+/-}$;*Rho*$^{REY/REY}$;*Gcaps*$^{-/-}$ (blue) rods were determined by measuring the dim-flash sensitivities at different wavelengths. (*C* and *D*) Averaged flash-response families in response to 10 ms 500 nm flashes at different light intensities and the intensity–response relations from 8 *Arr1*$^{+/G90D}$;*Rho*$^{REY/REY}$;*Gcaps*$^{-/-}$ rods (black) and 9 *Arr1*$^{+/-}$;*Rho*$^{REY/REY}$;*Gcaps*$^{-/-}$ rods (blue). The red curve in *D* is the intensity–response relation from *Rho*$^{WT/WT}$;*Gcaps*$^{-/-}$ rods obtained from our previous study (20). The intensity–response relations were fitted by a single saturating-exponential function giving half-saturating flash strengths of 6.21, 5,493, and 31,364 photons μm^{-2} for *Rho*$^{WT/WT}$;*Gcaps*$^{-/-}$, *Arr1*$^{+/G90D}$;*Rho*$^{REY/REY}$;*Gcaps*$^{-/-}$ and *Arr1*$^{+/-}$;*Rho*$^{REY/REY}$;*Gcaps*$^{-/-}$ rods, respectively. (*E*) Dim-flash responses of a *Arr1*$^{+/G90D}$;*Rho*$^{REY/REY}$;*Gcaps*$^{-/-}$ rod (black) and a *Arr1*$^{+/-}$;*Rho*$^{REY/REY}$;*Gcaps*$^{-/-}$ rod (blue) to repetitive 10 ms 500 nm flashes at 928.65 photons μm^{-2}. Stimuli that failed to elicit responses were labeled as "F" (a failure was defined as a flash trial that did not result in a response reaching a criterion amplitude, typically ≥50% of the single-photon-response peak within a characteristic time window based on the average response waveform). No failure was observed for *Arr1*$^{+/-}$;*Rho*$^{REY/REY}$;*Gcaps*$^{-/-}$ rods because of its small single-photon responses. (*F*) The average single-photon responses of *Rho*$^{WT/WT}$;*Gcaps*$^{-/-}$ (red), *Arr1*$^{+/G90D}$;*Rho*$^{REY/REY}$;*Gcaps*$^{-/-}$ (black), and *Arr1*$^{+/-}$;*Rho*$^{REY/REY}$;*Gcaps*$^{-/-}$ (blue) rods. n = 23 rods for *Rho*$^{WT/WT}$;*Gcaps*$^{-/-}$, 19 rods for *Arr1*$^{+/G90D}$;*Rho*$^{REY/REY}$;*Gcaps*$^{-/-}$, and 10 rods for *Arr1*$^{+/-}$;*Rho*$^{REY/REY}$;*Gcaps*$^{-/-}$.

(σ^2 = 0.178 ± 0.096 pA^2) was significantly higher than that in control *Arr1*$^{+/-}$;*Rho*$^{REY/REY}$;*Gcaps*$^{-/-}$ rods (σ^2 = 0.059 ± 0.028 pA^2), despite a similar dark current for the cells (Fig. 3 *A* and *B*). This noise resembled very much the noise shown by postbleach WT rods, in which the product, WT-Opsin, is known to trigger phototransduction intermittently via $G_{T1}\alpha$ (20). However, the continuous noise described here came from CSNB-causing mutant G90D-Rho rather than G90D-Opsin, because exogenous 11-*cis*-retinal had no effect on the continuous noise and dark current of *Arr1*$^{+/G90D}$;*Rho*$^{REY/REY}$;*Gcaps*$^{-/-}$ rods (*SI Appendix*, Fig. S1).

Table 1. Flash response parameters

Genotype	ROS length (μm)	I_{Dark} (pA)	S_F (pA photon^{-1} μm^2)	a (pA)	t_{int} (ms)	$\int f(t)dt$ (pC)	t_{peak} (ms)	τ_{rec} (ms)
Arr1$^{+/-}$;*Rho*$^{REY/REY}$;*Gcaps*$^{-/-}$	18.4 ± 1.0 (n = 30)	14.6 ± 1.3 (n = 8)	(3.57 ± 0.77) × 10^{-4} (n = 12)	0.17 ± 0.06 (n = 9)	1,185 ± 142 (n = 9)	0.203 ± 0.076 (n = 9)	771 ± 128 (n = 9)	418 ± 62 (n = 9)
Arr1$^{+/G90D}$;*Rho*$^{REY/REY}$;*Gcaps*$^{-/-}$	18.8 ± 1.2 (n = 28)	15.4 ± 2.2 (n = 8)	(1.41 ± 0.55) × 10^{-3} (n = 19)	2.8 ± 0.9 (n = 19)	777 ± 120 (n = 19)	2.16 ± 0.85 (n = 19)	528 ± 96 (n = 19)	354 ± 111 (n = 19)

Values are mean ± SD, with the number of cells analyzed (n) in parentheses. Rod outer segment (ROS) length is the approximate length of live rod outer segments measured with light microscopy. Flash responses were measured from calibrated 10 ms flashes at 500 nm. I_{Dark} is the maximum response amplitude representing the dark current; S_F is the flash sensitivity; a is the single-photon response amplitude; t_{int} and t_{peak} are the integration time and time-to-peak of dim-flash responses, respectively; $\int f(t)dt$ is the time integral of single-photon responses. τ_{rec} is the recovery time constant obtained from exponential fits to the final decay of dim-flash responses.

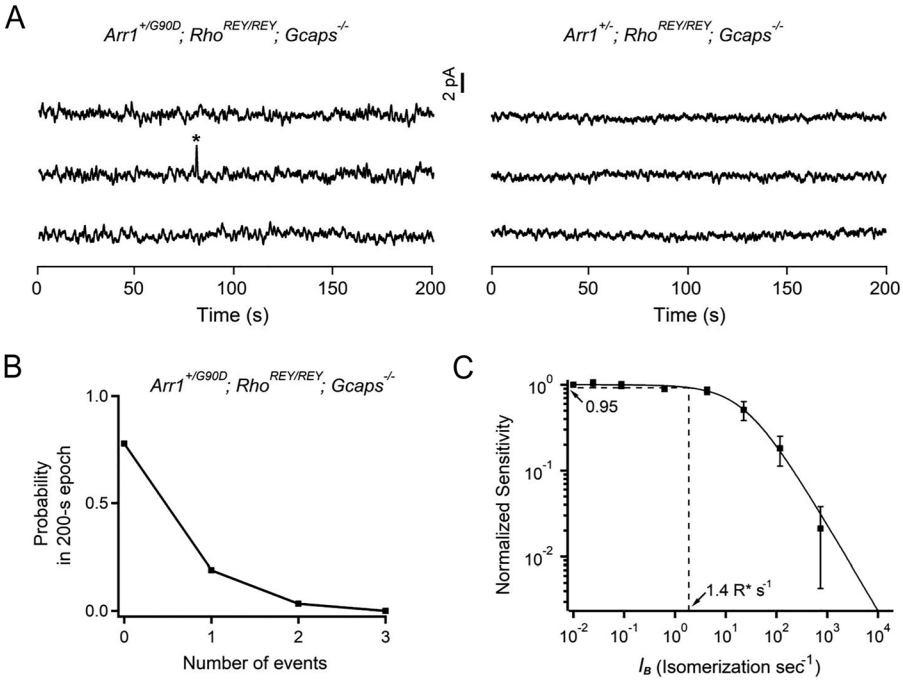

Fig. 2. Dark quantal noise from *Arr1*$^{+/G90D}$*;Rho*$^{REY/REY}$*;Gcaps*$^{-/-}$ rods. (*A*) 10-min dark noise recordings from *Arr1*$^{+/G90D}$*;Rho*$^{REY/REY}$*;Gcaps*$^{-/-}$ and *Arr1*$^{+/-}$*;Rho*$^{REY/REY}$*;Gcaps*$^{-/-}$ rods with the spontaneous isomerization events labeled with stars. (*B*) Poisson analysis of the spontaneous isomerization events collected from all *Arr1*$^{+/G90D}$*;Rho*$^{REY/REY}$*;Gcaps*$^{-/-}$ rods. The probability of 0, 1, 2, and 3 events observed in a total of 90 trials of 200-s epochs is plotted as the square symbols. The solid line shows very good fit by the Poisson distribution with a mean event rate of 0.0013 s^{-1}. (*C*) Weber–Fechner relation of WT rods. Data replotted from ref. 21. Weber–Fechner relation [$S_F/S_F^D = 1/(1 + I_B/I_O)$] fit to flash sensitivity (S_F) normalized to dark adapted sensitivity (S_F^D) plotted against background light. (I_B, converted to isomerizations s^{-1} by multiplying with the effective collective area of mouse rods, ~0.4 μm^2.) The intensity required to reduce sensitivity by half (Io) was 63 photons μm^{-2} s^{-1} (~24 isomerizations s^{-1}).

We first wanted to know whether the G90D-Rho-generated continuous noise required its downstream G-protein, transducin. Accordingly, we bred the *Arr1*$^{+/G90D}$*;Rho*$^{REY/REY}$*;Gcaps*$^{-/-}$ mouse line into a *Gnat1*$^{-/-}$*;Gnat1*^{Tg} background, where rod transducin ($G_{T1}\alpha$) is expressed at ~6% of *WT* (20). As a result, the continuous noise of *Arr1*$^{+/G90D}$*;Rho*$^{REY/REY}$*;Gcaps*$^{-/-}$*;Gnat1*$^{-/-}$*;Gnat1*^{Tg} rods was drastically reduced, with a variance down to $\sigma^2 = 0.055 \pm 0.013$ pA^2 (Fig. 3 *C*, *Left Top* and Fig. 3 *D*, *Right*), close to that of *Arr1*$^{+/-}$*;Rho*$^{REY/REY}$*;Gcaps*$^{-/-}$ rods lacking G90D-Rho (Fig. 3*B*), again with no change in dark current. Conversely, knocking-out RGS9 (*Arr1*$^{+/G90D}$*;Rho*$^{REY/REY}$*;Gcaps*$^{-/-}$*;RGS9*$^{-/-}$), a protein that accelerates the hydrolysis of the GTP bound to the active $G_{T1}\alpha^*$ and consequently prolonging the active lifetime of $G_{T1}\alpha^*$ and hence phototransduction (23, 24), the continuous noise was further increased (Fig. 3 *C*, *Left Bottom* and Fig. 3 *D*, *Right*). Thus, G90D-Rho-triggered dark continuous noise went through $G_{T1}\alpha$, and the underlying unitary response should be representable by the electrical response evoked by a single $G_{T1}\alpha^*$·PDE* complex—essentially the same as the electrical response produced by a single transiently active WT-Opsin molecule (20). Previously, we obtained the power spectrum of the latter from the dark continuous noise associated with WT-Opsin produced after a bleach, describable by a convolution of two single-exponential declines, with time constants of $\tau_1 = 81 \pm 35$ ms, $\tau_2 = 231 \pm 25$ ms (20). As such, by calculating the power spectra of continuous noise in *Arr1*$^{+/G90D}$*;Rho*$^{REY/REY}$*;Gcaps*$^{-/-}$ and in *Arr1*$^{+/-}$*;Rho*$^{REY/REY}$*;Gcaps*$^{-/-}$ rods, and taking the difference between them (difference spectrum), we found the result to indeed match the activity of the single rod transducin ($G_{T1}\alpha^*$·PDE*) (Fig. 3 *F* and *G*). Thus, the activity underlying the dark continuous noise triggered by G90D-Rho is identical in waveform to that triggered by WT-opsin after a bleach, with each being the unitary $G_{T1}\alpha^*$·PDE* response.

Overall Adapting Effect of G90D-Rho Constitutive Noise. The paradigm of visual adaptation is typically in the context of a reduction in dim-flash sensitivity by a steady background light of increasing intensity. In our situation, we shall need to start with the intrinsic noise coming from G90D-Rho measured initially at a low expression level (0.1% G90D-Rho) in order to resolve the noise, then to extrapolate to a much higher expression level corresponding to CSNB disease. In this extrapolation, the driver of the adaptation can be in the form of an equivalent steady background light intensity or in the form of a steady mean response resulting from the background light stimulus. Because the overall G90D-Rho intrinsic noise that we have measured consisted of a combination of spontaneous-isomerization noise in units of R* s^{-1} (equivalent steady-light intensity) and continuous noise in units of pA (mean steady-response amplitude), it is much more convenient to adhere to the same unit for both, R* s^{-1}. The Weber–Fechner relation describing background adaptation is commonly written as (equation 22 in ref. 25):

$$\frac{S_F}{S_F^D} = \frac{I_O}{I_O + I_B}, \qquad [1]$$

where S_F is flash sensitivity in the presence of a background light I_B, S_F^D is flash sensitivity in the absence of background light (i.e., in darkness), and I_O is the background intensity that reduces the flash sensitivity in darkness by half. The important point to note is that in Eq. **1**, which is actually a simple empirical fit to background-adaptation data, I_B is a parameter that increases linearly with background light intensity (and also with equivalent background intensity), whereas steady mean response does not increase linearly with intensity because of response compression (see ref. 26). In the following, we provide calculations to express both kinds of mutant-pigment constitutive activities in units of

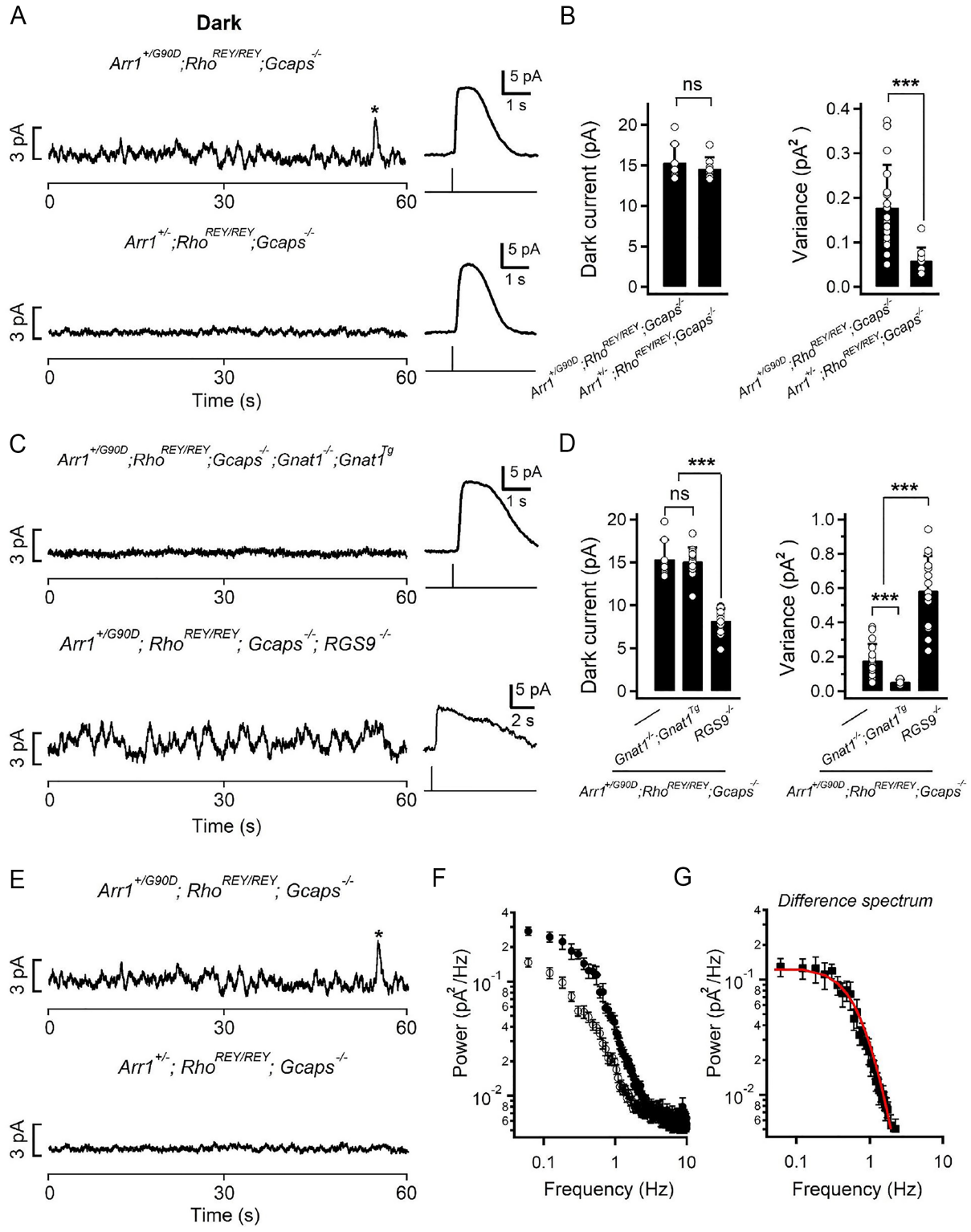

Fig. 3. Dark continuous noise from G90D-Rho. (*A*) 60-s dark noise recordings (*Left*) and saturated light responses to 10 ms 500 nm flashes (*Right*) from *Arr1*$^{+/G90D}$;*Rho*$^{REY/REY}$;*Gcaps*$^{-/-}$ and *Arr1*$^{+/-}$;*Rho*$^{REY/REY}$;*Gcaps*$^{-/-}$ rods. The saturated light intensities were 85,958 and 305,869 photons μm^{-2} for *Arr1*$^{+/G90D}$;*Rho*$^{REY/REY}$;*Gcaps*$^{-/-}$ and *Arr1*$^{+/-}$;*Rho*$^{REY/REY}$;*Gcaps*$^{-/-}$ rods, respectively. (*B*) Statistics for the dark current and variance of continuous noise of *Arr1*$^{+/G90D}$;*Rho*$^{REY/REY}$;*Gcaps*$^{-/-}$ and *Arr1*$^{+/-}$;*Rho*$^{REY/REY}$;*Gcaps*$^{-/-}$ rods in *A*. The continuous noise is defined as dark noise without showing any spontaneous isomerization events. n = 8 rods for the dark current and 22 rods for the variance of *Arr1*$^{+/G90D}$;*Rho*$^{REY/REY}$;*Gcaps*$^{-/-}$, 9 rods for the dark current and 12 rods for the variance of *Arr1*$^{+/-}$;*Rho*$^{REY/REY}$;*Gcaps*$^{-/-}$. (*C*) 60-s dark noise recordings (*Left*) and saturated light responses to 10 ms 500 nm flashes (*Right*) from *Arr1*$^{+/G90D}$;*Rho*$^{REY/REY}$;*Gcaps*$^{-/-}$;*Gnat1*$^{-/-}$;*Gnat1*^{Tg} and *Arr1*$^{+/G90D}$;*Rho*$^{REY/REY}$;*Gcaps*$^{-/-}$;*RGS9*$^{-/-}$ rods. The saturated light intensities were 1,176,206, and 41,546 photons μm^{-2} for *Arr1*$^{+/G90D}$;*Rho*$^{REY/REY}$;*Gcaps*$^{-/-}$;*Gnat1*$^{-/-}$;*Gnat1*^{Tg} and *Arr1*$^{+/G90D}$;*Rho*$^{REY/REY}$;*Gcaps*$^{-/-}$;*RGS9*$^{-/-}$ rods, respectively. (*D*) Statistics for the dark current and variance of continuous noise in *C*. n = 15 rods for either the dark current or the variance of *Arr1*$^{+/G90D}$;*Rho*$^{REY/REY}$;*Gcaps*$^{-/-}$;*Gnat1*$^{-/-}$;*Gnat1*^{Tg}, 15 rods for either the dark current or the variance of *Arr1*$^{+/G90D}$;*Rho*$^{REY/REY}$;*Gcaps*$^{-/-}$;*RGS9*$^{-/-}$. (*E*) 60-s dark-noise recordings from *Arr1*$^{+/G90D}$;*Rho*$^{REY/REY}$;*Gcaps*$^{-/-}$ and *Arr1*$^{+/-}$;*Rho*$^{REY/REY}$;*Gcaps*$^{-/-}$rods as in *A*. (*F*) Averaged continuous-noise power spectra from 22 *Arr1*$^{+/G90D}$;*Rho*$^{REY/REY}$;*Gcaps*$^{-/-}$ (closed circles) and 12 *Arr1*$^{+/-}$;*Rho*$^{REY/REY}$;*Gcaps*$^{-/-}$(open circles) rods. Each frequency point indicates mean ± SEM. (*G*) Difference spectrum obtained by subtracting the power spectrum of *Arr1*$^{+/-}$;*Rho*$^{REY/REY}$;*Gcaps*$^{-/-}$rods from the power spectrum of *Arr1*$^{+/G90D}$;*Rho*$^{REY/REY}$;*Gcaps*$^{-/-}$ rods was fitted by the waveform of single transducin response (red curve). Statistical data are presented as mean ± SD. Statistical significance was analyzed by Student's *t* test for *B* or one-way ANOVA for *D*, ***$P < 0.001$; ns, not significant.

equivalent R* s^{-1}, thus allowing them to summate in a linear fashion regardless of intensity.

For unitary events with waveform *f(t)* occurring randomly at a mean rate of ν s^{-1}, the mean and the variance of the steady signal resulting from such events are given by Campbell's Theorems (27–29):

$$\text{Steady–noise mean } (m) = \nu \int f(t)dt, \quad [2]$$

$$\text{Steady–noise variance } (\sigma^2) = \nu \int \left[f(t)\right]^2 dt, \quad [3]$$

Eqs. **2** and **3** are often used together in situations where $f(t)$ is a priori unknown. In the present case, however, *f(t)* is known from prior work.

For spontaneous isomerizations originating from G90D-Rho expressed in *Arr1*$^{+/G90D}$*;Rho*$^{REY/REY}$*;Gcaps*$^{-/-}$ rods at ~0.1% of normal (i.e., 0.1% WT-Rho in WT rods), the rate was measured to be 0.0014 R* s^{-1} $cell^{-1}$ (see earlier section). The time integral of the single-photon response, $f_i(t)$ (where subscript "*i*" denotes isomerization noise, and $f_i(t)$ was measured in *Gcaps*$^{-/-}$ background), generated by G90D-Rho, is given by $\int f_i(t)dt$ = 2.16 pC (Table 1 and legend). Thus, applying Eq. **2**, the steady-noise mean, m_i, from G90D-Rho-triggered isomerization noise is given by ν_i $\int f_i(t)dt$ = 0.0014 s^{-1} × 2.16 pC = 0.003 pA.

G90D-Rho-triggered continuous noise in darkness was shown to comprise random unitary electrical events each being triggered by a single $G_{T1}\alpha^*$·PDE* complex (see earlier section). Our previous work on dark continuous noise after a bleach has provided the waveform kinetics (see earlier) as well as the transient peak amplitude (0.27 pA on average; ref. 20) of the response evoked by a single $G_{T1}\alpha^*$·PDE* complex (20). Thus, the time integral of the unitary event underlying G90D-Rho-triggered continuous noise, $\int f_c(t)dt$, can be calculated to be 0.12 pC (20), and $\int \left[f_c(t)\right]^2 dt$ calculated to be 0.021 pA^2 s (where subscript "*c*" denotes continuous noise) after averaging values for the unitary $G_{T1}\alpha^*$·PDE*-driven responses under different bleaching conditions in a previous study (20). Next, between the *Arr1*$^{+/G90D}$*;Rho*$^{REY/REY}$*;Gcaps*$^{-/-}$ genotype and the *Arr1*$^{+/-}$*;Rho*$^{REY/REY}$*;Gcaps*$^{-/-}$ genotype, their difference in continuous-noise variance gave the G90D-Rho-triggered continuous-noise variance; i.e., $\sigma_c^2 = \sigma^2$*Arr1*$^{+/G90D}$*;Rho*$^{REY/REY}$*;Gcaps*$^{-/-}$ - σ^2*Arr1*$^{+/-}$*;Rho*$^{REY/REY}$*;Gcaps*$^{-/-}$ = 0.178 pA^2 – 0.059 pA^2 = 0.119 pA^2. Thus, from Eq. **3**, the frequency, ν_c, of unitary events comprising G90D-Rho continuous noise at 0.1% expression of G90D-Rho, is given by $\nu_c = \sigma_c^2/\{\int [f_c(t)]^2 dt\}$ = 0.119 pA^2/0.021 pA^2 s ~5.67 s^{-1}. Inserting this ν_c value into Eq. **2**, we obtained a steady-noise mean for G90D-Rho-triggered continuous noise, $m_c = \nu_c \int f_c(t)dt$ = 5.67 s^{-1} × 0.12 pC = 0.68 pA. Comparing this value to a mean steady current of only 0.003 pA (see above) caused by the spontaneous isomerization of G90D-Rho at 0.1% expression, the continuous noise is therefore 0.68 pA/0.003 pA, or ~230-fold as high or effective. Converting this parameter into equivalent background light, this gives 230 × 0.0014 R* s^{-1} $cell^{-1}$ = ~0.32 R* s^{-1} $cell^{-1}$, for ~0.1% of G90D-Rho expression. Thus, 100% of G90D-Rho holo-pigment should produce ~320 R* s^{-1} $cell^{-1}$ for dark continuous noise, which is ~40,000-fold as high as the spontaneous-isomerization rate of 100% WT-Rho (0.008 ± 0.004 R* s^{-1} $cell^{-1}$; ref. 21).

Predicting Macroscopic G90D-Rho CSNB Phenotype Based on Constitutive Activity from Lowly Expressed (0.1%) G90D-Rho. It would be useful to know whether our detailed analysis of the lowly expressed G90D-Rho constitutive noise as described above is able to predict the overall phenotype as shown by a KI mouse model in the condition of the CSNB disease found in human patients. Accordingly, we used CRISPR/Cas9 to generate heterozygous *Rho*$^{G90D/WT}$ and homozygous *Rho*$^{G90D/G90D}$ KI mouse lines. Histological data from these lines showed very minor retinal degeneration at 1-mo old of age in comparison to *Rho*$^{WT/WT}$ (*SI Appendix*, Fig. S2), consistent with the CSNB phenotype (5). Next, we quantified with spectrophotometry the amounts of WT-Rho and G90D-Rho proteins from *Rho*$^{WT/WT}$, *Rho*$^{G90D/WT}$, and *Rho*$^{G90D/G90D}$ mouse retinae that had been solubilized. Fig. 4*A* shows, successively, i) the spectrum in darkness (black trace), ii) the spectrum after treatment with hydroxylamine in darkness (blue trace), and iii) the spectrum after bleaching with light (yellow trace). WT-Rho is resistant to hydroxylamine treatment in darkness (Fig. 4 *A*, *Left*), whereas G90D-Rho is bleachable by hydroxylamine even in darkness (Fig. 4 *A*, *Right*), yielding G90D-opsin and the stable retinal oxime with a λ_{max} at 367 nm (9, 15). The amount of WT-Rho in *Rho*$^{WT/WT}$ retinae and G90D-Rho in *Rho*$^{G90D/G90D}$ retinae were determined by subtracting the spectrum after bleaching (yellow traces in Fig. 4 *A*, *Left* and *Right*) from the spectrum in the dark (black traces in Fig. 4 *A*, *Left* and *Right*). In the case of *Rho*$^{G90D/G90D}$ retinae, the traces for light-bleached or hydroxylamine-bleached were identical, as expected. For *Rho*$^{G90D/WT}$ retinae, expressing both WT and G90D-Rho, we first measured the amount of G90D-Rho by subtracting the spectrum after hydroxylamine treatment (blue trace in Fig. 4 *A*, *Middle*) from the spectrum in the dark (black trace in Fig. 4 *A*, *Middle*), and then the amount of WT-Rho by subtracting the spectrum after bleaching (yellow trace in Fig. 4 *A*, *Middle*) from the spectrum after hydroxylamine treatment (blue trace in Fig. 4 *A*, *Middle*). Our final measurements indicated that the amounts of G90D-Rho in *Rho*$^{G90D/WT}$ and *Rho*$^{G90D/G90D}$ retinae were 0.13 ± 0.032 nmol/retina, and 0.38 ± 0.031 nmol/retina (Table 2), respectively. Compared to the amount of WT-Rho in *Rho*$^{WT/WT}$ retinae (0.52 ± 0.018 nmol/retina, Table 2), the expression level of G90D-Rho in *Rho*$^{G90D/WT}$ and *Rho*$^{G90D/G90D}$ retinae was 0.13/0.52 = 25% and 0.38/0.52 = ~70%, respectively.

The level of G90D-Rho (0.13 ± 0.032 nmol/retina) was significantly lower than that of WT-Rho (0.20 ± 0.0070 nmol/retina, $P < 0.01$, Table 2) in *Rho*$^{G90D/WT}$ rods. To see whether this difference reflects a difference in transcript levels from the WT-Rho and G90D-Rho allele, we performed reverse transcription-PCR and used PCR primers to amplify a common fragment of rhodopsin cDNA from both alleles. The G90D-Rho KI mutation abolished a BbsI restriction site within this fragment. Accordingly, the PCR fragment was digested with BbsI to distinguish WT-Rho and G90D-Rho transcripts (*SI Appendix*, Fig. S3). The intensity of the uncut and cut fragments was quantified using Fiji (ImageJ), and the results show 56 ± 4% (mean ± SD, N = 5 retinae) of the transcript belonging to G90D in *Rho*$^{G90D/WT}$ retinae, a value close to 50% transcript derived from one allele. The relatively lower G90D-Rho protein level in *Rho*$^{G90D/WT}$ compared to WT-Rho as well as in *Rho*$^{G90D/G90D}$ (~70% of WT-Rho) suggests that the G90D-Rho is slightly less stable than WT-Rho pigment.

Thus, based on the above calculations that 100% of G90D-Rho would produce an equivalent background light of ~320 R* s^{-1} $cell^{-1}$ for dark continuous noise and of ~1.4 R* s^{-1} $cell^{-1}$ for spontaneous isomerization, the equivalent background light from G90D-Rho in *Rho*$^{G90D/WT}$ rods, being at 25% expression, would be 320 R* s^{-1} $cell^{-1}$ × 25% = 80 R* s^{-1} $cell^{-1}$ for continuous noise and 1.4 R* s^{-1} $cell^{-1}$ × 25% = 0.35 R* s^{-1} $cell^{-1}$ for spontaneous isomerization, or a total of ~80.4 R* s^{-1} $cell^{-1}$. In *Rho*$^{G90D/G90D}$ rods, being at ~70% expression, the equivalent background light from G90D-Rho would be 320 × 70% = 224 R* s^{-1} $cell^{-1}$ for

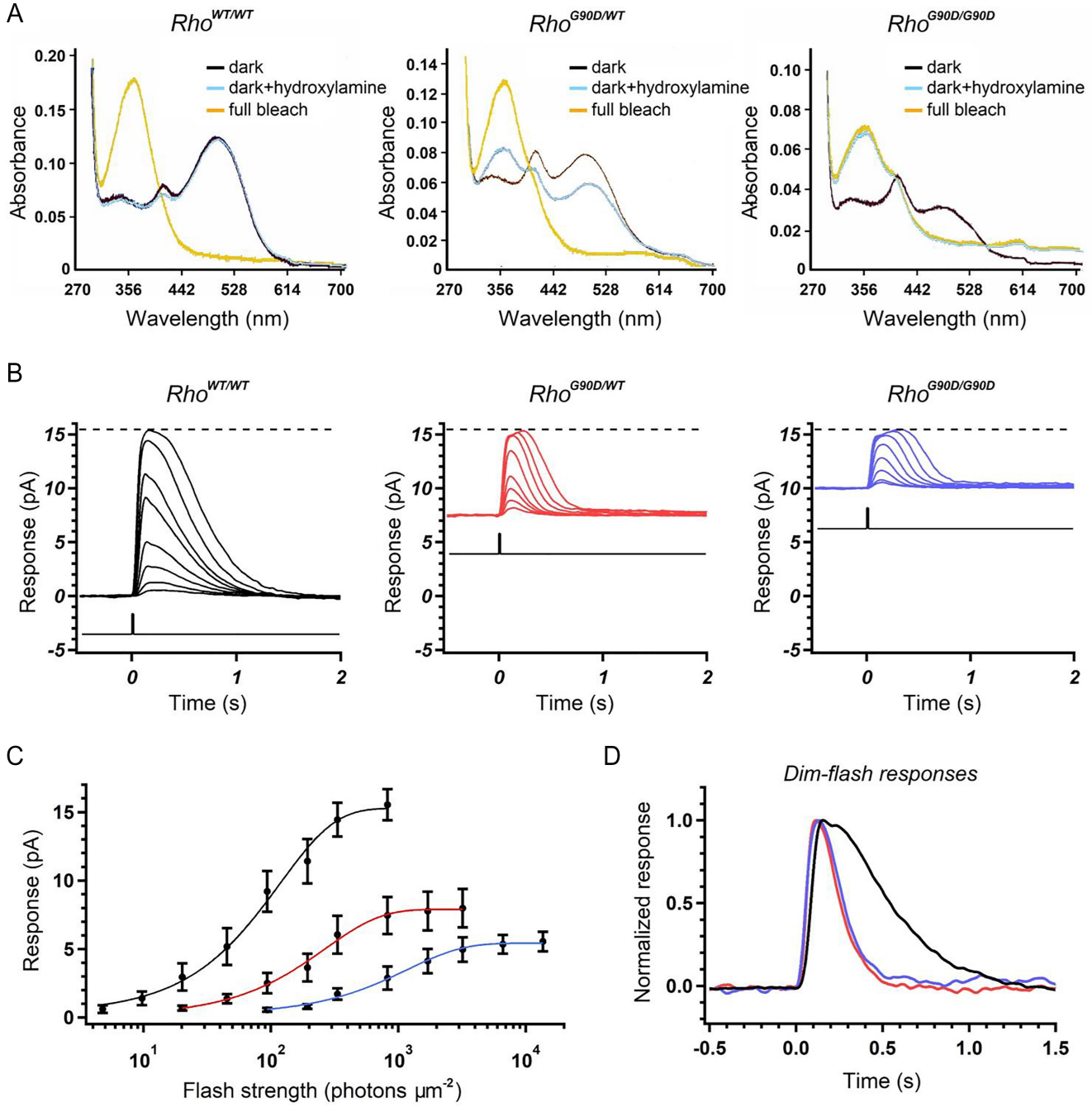

Fig. 4. Loss of rod sensitivity in KI mice carrying G90D-Rho point mutation. (*A*) Absorption spectrum of a $Rho^{WT/WT}$ (*Left*), a $Rho^{G90D/WT}$ (*Middle*), or a $Rho^{G90D/G90D}$ (*Right*) retina first in the dark (black trace), then treatment of hydroxylamine in darkness (blue trace), followed with light bleaching (yellow trace). (*B* and *C*) Averaged flash-response families in response to 10 ms 500 nm flashes at different light intensities and the intensity–response relations from $Rho^{WT/WT}$ (black), $Rho^{G90D/WT}$ (red), and $Rho^{G90D/G90D}$ rods (blue). The intensity–response relations were fitted by single saturating-exponential functions. n = 10 rods for each genotype. (*D*) Averaged dim-flash responses of $Rho^{WT/WT}$ (black), $Rho^{G90D/WT}$ (red), and $Rho^{G90D/G90D}$ rods (blue). The faster kinetics of the dim-flash responses in $Rho^{G90D/WT}$ and $Rho^{G90D/G90D}$ rods indicates background light adaptation in the $Rho^{G90D/WT}$ and $Rho^{G90D/G90D}$ rods.

continuous noise and 1.4 $R^* s^{-1}$ $cell^{-1}$ × 70% = 0.98 $R^* s^{-1}$ $cell^{-1}$ for spontaneous isomerization, giving a total of ~225 $R^* s^{-1}$ $cell^{-1}$. In Fig. 4*B*, we plotted the averaged absolute dark-current amplitudes of $Rho^{WT/WT}$, $Rho^{G90D/WT}$, and $Rho^{G90D/G90D}$ rods, at ~15 pA, 8 pA, and 5 pA, respectively, superposed over which are averaged flash-response families (with transient peak amplitudes plotted against log flash intensities shown in Fig. 4*C*). The flash sensitivity in each genotype was calculated at the lowest flash intensity, giving values of 0.12 ± 0.04 pA $photon^{-1}$ μm^2 for $Rho^{WT/WT}$ rods, 0.027 ± 0.0080 pA $photon^{-1}$ μm^2 for $Rho^{G90D/WT}$ rods and 0.0059 ± 0.0013 pA $photon^{-1}$ μm^2 for $Rho^{G90D/G90D}$ rods (Table 3). After normalization against the flash sensitivity in $Rho^{WT/WT}$ rods, the dim flash responses in $Rho^{G90D/WT}$ rods and $Rho^{G90D/G90D}$ rods were, respectively, 4.4-fold lower in $Rho^{G90D/WT}$ rods and 20.3-fold lower in $Rho^{G90D/G90D}$ rods—broadly similar to those previously obtained in heterozygous $Rho^{G90D+};Rho^{WT/+}$ and homozygous $Rho^{G90D+/+};Rho^{-/-}$ rods containing the G90D-Rho transgene (9, 12)—resulting from the intrinsically high constitutive activity. Not only was the dim-flash sensitivity much lower due to the G90D-Rho constitutive activity, the decay of the response to test flashes was also accelerated (Fig. 4*D*), as expected from the equivalent-background light adaptation.

Table 2. Rhodopsin amount measured by spectrophotometry

Genotype	WT-Rho (nmol/retina)	G90D-Rho (nmol/retina)	Total (nmol/retina)
(1) *Rho*$^{WT/WT}$(1 mo)	0.52 ± 0.018 (n = 3)	NA (n = 3)	0.52 ± 0.018 (n = 3)
(2) *Rho*$^{G90D/WT}$(1 mo)	0.20 ± 0.0070 (n = 6)	0.13 ± 0.032 (n = 6)	0.34 ± 0.036 (n = 6)
(3) *Rho*$^{G90D/G90D}$(1 mo)	NA (n = 3)	0.38 ± 0.031 (n = 3)	0.38 ± 0.031 (n = 3)

Values are mean ± SD, with the number of cells analyzed (n) in parentheses. Absorbance at 500 nm (WT-Rho; 46,000 M^{-1} cm^{-1}). Absorbance at 484 to 496 nm (G90D-Rho, 37,000 M^{-1} cm^{-1}).

In Fig. 5*A*, we have overlaid on the standard mouse Weber–Fechner relation (dashed curve, reproduced from Fig. 2*C*) the relative flash sensitivities (red crosses) from the heterozygous KI *Rho*$^{G90D/WT}$ rods and the homozygous *Rho*$^{G90D/G90D}$ rods measured above, together with the expected corresponding equivalent background light intensities extrapolated from the G90D-Rho constitutive activities at 0.1% expression to 25% and 70% expression, respectively. It can be seen that the behavior of the CSNB rods is remarkably close to that predicted from these equivalent background lights based on the Weber–Fechner relation. In fact, the match between measurement and prediction is remarkably good—at 25% G90D-Rho expression, the red cross is almost spot on, while at 70% expression, the equivalent I_B is also within a factor of two from the Weber–Fechner curve—because any measurement error in the mutant-pigment constitutive activities would have been substantially amplified by the extended extrapolation over 250- to 700-fold. Not only was the correlation between sensitivity and constitutive activity excellent, but the dim-flash response kinetics behaved as expected as well, in that the speeding up of response decay was very similar (compare between red and black traces in Fig. 5 *B*, *Top* and between blue and black traces in Fig. 5 *B*, *Bottom*) regardless of whether the adaptation came from G90D-Rho constitutive activity in *Rho*$^{G90D/WT}$and *Rho*$^{G90D/G90D}$ mice, or from authentic steady light at the appropriate intensities on *Rho*$^{WT/WT}$ mice (Fig. 5*B*).

Discussion

CSNB is an inherited retinal disease known to cause sensitivity loss of rod vision in scotopic light while sparing cone vision under photopic light (3, 4). It can be caused by genetic mutations affecting proteins that deactivate rhodopsin, leading to constitutive activation of the phototransduction cascade. These include GRK1 (30) and ARR1 (31) loss-of-function mutations found in patients diagnosed with Oguchi disease. Four rhodopsin mutations (G90D, T94I, A292E, and A295V) have been associated with CSNB due to their higher-than-normal dark constitutive activities (6–12). One key problem in the studies published so far, at least with G90D-Rho, has been that adaptation by the host cell to the equivalent background light coming from the constitutive activity of the mutant rhodopsin is so strong that it is impossible to resolve the nature of the adapting constitutive activity. In the present study, we have gotten around this problem by expressing the mutant G90D-Rho causing CSNB at such a low level (~0.1% of WT-Rho in WT animals) that the resulting adaptation by the host cell remained weak enough to allow resolution of the constitutive activity of G90D-Rho. At this low G90D-Rho expression level, we were able to observe two types of constitutive activities. The first was spontaneous isomerization of G90D-Rho, occurring at 0.0014 R* s^{-1}, equivalent to 175 times of the normal rate if it were expressed at 100%. Although this fold-increase caused by disease is high, the actual absolute constitutive activity remains miniscule, equivalent to only 1.4 R* s^{-1}, causing hardly any adaptation in the host cell at all (*Results*). The second was a continuous noise, consisting of a high frequency of unitary electrical events each triggered by a single $G_{T1}\alpha$*·PDE* complex. Even though these events were of low amplitude (0.27 pA) at transient peak, they occurred at such a high frequency that, if G90D-Rho were expressed at the level of 100% in the mouse, the event rate would be 5.67 s^{-1} × (100/0.1) = 5,670 s^{-1}, or equivalent to a steady background light of about 320 R* s^{-1} (*Results*), which is very high. When summed together with the spontaneous isomerization of 1.4 R* s^{-1}, the overall equivalent background light would be 321.4 R* s^{-1} at 100% G90D expression. At this point, it is not certain whether the other three rhodopsin point mutants (T94I, A292E, and A295V) also cause CSNB in the same manner. We are currently generating similar KI mouse lines expressing these other rhodopsin mutants at both low and disease-state levels to examine whether this is the case.

The most interesting finding in the present work is that the major cause of CSNB, at least in the case of G90D-Rho, is actually constitutive low-amplitude noise from G90D-Rho instead of spontaneous isomerization from G90D-Rho or other activity from G90D-Opsin, with the latter being ruled out by the lack of any effect of exogenous 11-*cis*-retinal on the resulting desensitization in the CSNB mouse rods (*SI Appendix,* Fig. S4 and ref. 12). As such, the most recent work by Dizhoor et al. (12) did come closest to our findings, although this group failed to resolve the constitutive activity in darkness.

The mechanism by which G90D-Rho leads to two kinds of constitutive activity remains a mystery at present. In WT-Rho, the salt bridge formed between E113 and K296 is a key constraint for maintaining the basal state of the pigment (13, 16). The G90D mutation introduces an aspartic acid that competes with E113 for forming the salt bridge with K296 and interferes with covalent bonding with the chromophore. This interference with the site of chromophore attachment may explain the increased rate of thermal isomerization that we observed. With respect to the continuous noise, it may be of relevance that spin-label experiments combined with electron paramagnetic resonance showed that G90D-Rho can adopt an active dark state that is strikingly similar to light-activated WT-Rho (32). This preactive conformation is also supported by liquid-state NMR (33), FTIR (34), and dynamic single-molecule force spectroscopy (15) experiments. Additionally, whereas 11-*cis*-retinal forms a network of intramolecular interactions that greatly stabilizes dark

Table 3. Flash response parameters

Genotype	I_{Dark} (pA)	S_F (pA photon^{-1} μm^2)	t_{int} (ms)	t_{peak}(ms)	τ_{rec}(ms)
(1) *Rho*$^{WT/WT}$(1 mo)	15.54 ± 1.14 (n = 10)	0.12 ± 0.04 (n = 10)	405 ± 70 (n = 10)	162 ± 46 (n = 10)	224 ± 25 (n = 10)
(2) *Rho*$^{G90D/WT}$(1 mo)	8.02 ± 1.43 (n = 11)	0.027 ± 0.0080 (n = 10)	214 ± 46 (n = 10)	114 ± 18 (n = 10)	109 ± 32 (n = 10)
(3) *Rho*$^{G90D/G90D}$(1 mo)	5.55 ± 0.70 (n = 10)	0.0059 ± 0.0013 (n = 10)	227 ± 41 (n = 10)	127 ± 31 (n = 10)	107 ± 31 (n = 10)

Values are mean ± SD, with the number of cells analyzed (n) in parentheses. Flash responses were measured from calibrated 10 ms flashes at 500 nm for *Rho*$^{WT/WT}$, *Rho*$^{G90D/WT}$, and *Rho*$^{G90D/G90D}$. I_{Dark} is the maximum response amplitude representing the dark current; S_F is the flash sensitivity; t_{int} and t_{peak} are the integration time and time-to-peak of dim-flash responses, respectively; τ_{rec} is the recovery time constant obtained from exponential fits to the final decay of dim-flash responses.

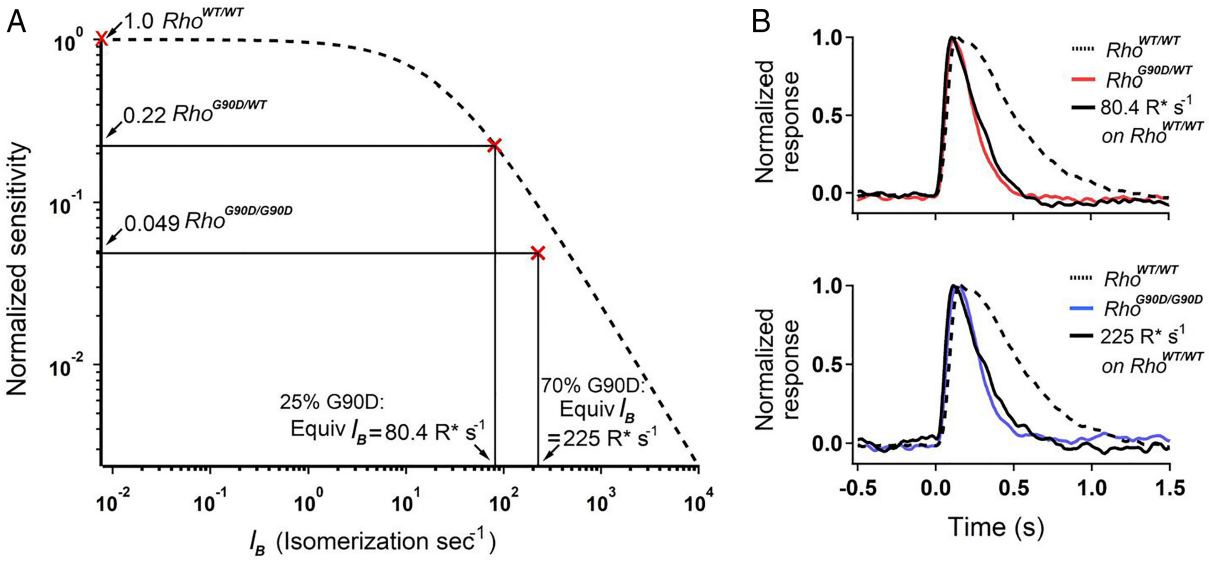

Fig. 5. Prediction of rod sensitivity for $Rho^{G90D/WT}$ and $Rho^{G90D/G90D}$ mice. (*A*) Weber–Fechner relation of WT rods shown earlier in Fig. 2*C*. The three crosses indicate the normalized dim-flash sensitivity of $Rho^{WT/WT}$, $Rho^{G90D/WT}$, and $Rho^{G90D/G90D}$ rods against the equivalent background light of 0, 80.4, and 225 R* s^{-1}, respectively. (*B*) Comparison of the dim-flash waveforms from $Rho^{G90D/WT}$ (red trace in *Upper* panel) and $Rho^{G90D/G90D}$ (blue trace in *Lower* panel) rods with that from $Rho^{WT/WT}$ rods under background light intensities equivalent to 80.4 and 225 R* s^{-1} (solid black traces), respectively. The dim-flash waveform for dark-adapted $Rho^{WT/WT}$ rods was shown as dashed black trace.

WT-Rho, G90D-Rho is not stabilized by 11-*cis*-retinal (10). Despite these differences, dark G90D-Rho does not have increased basal activity within the detection limit of in vitro G-protein activation assay (14, 32), indicating that some structural constraints remain. Together, these studies provide evidence that the constraints on dark G90D-Rho may be weaker than that on WT-Rho, and this weakened intramolecular network may underlie the continuous noise that we measured using suction-electrode recordings.

The question remains what makes a mutant rhodopsin with constitutive activity in darkness trigger CSNB versus RP? Structural studies of G90D combined with modeling of other CSNB mutants (T94I, A292E, and A295V) show that they share a common theme of specific interactions with K296 (16). These interactions may explain why these mutants fold well and form a visual pigment. In contrast to G90D, the G90V mutation, which leads to RP, does not favor similar interactions with K296 (16). In a general case in which a pigment's constitutive activity and RP are known to coexist, it may require closer scrutiny to interrogate any correlation between the two. One such example is D190N-Rho, a rhodopsin mutant with a higher-than-normal constitutive activity (spontaneous isomerization) due to a defective chromophore-binding pocket (21) and also known to cause RP. When we examined spontaneous isomerization from rods harboring D190N-Rho, we found a 16-fold increase in its activity from normal. However, upon assay of the D190N-Rho expression level, it turned out to be lower than normal, thus providing compensation for D190N-Rho's higher constitutive activity. In the same work, we found that the diseased RP symptoms in D190N-Rho rods actually came from a misfolded protein response, an issue separate from constitutive activity. Separately, we also found that much of the degeneration of $Rho^{D190N/WT}$ mouse rods was not averted by genetically deleting Gnat1, thus dissociating the two phenomena. As such, one functional way to check the relevance of constitutive activity to RP would be to ask whether the $Gnat1^{-/-}$ genotype removes the signs of RP (21). In contrast to D190N, G90D-Rho folds well and signals through transducin. A comparison of WT-Rho and G90D-Rho in $Rho^{G90D/WT}$ heterozygous mice shows a small but significant lowered level of G90D-Rho (Table 2), indicating a slight structural instability which may contribute to slow retinal degeneration over time. Constitutive activity can also drive cell death (31, 35), as some CSNB patients do progress to RP (36). Identification of these mechanisms provides future targets for therapeutic interventions.

Materials and Methods

All experiments were conducted according to the protocols approved by the Institutional Animal Care and Use Committee at Johns Hopkins University. The G90D-Rho KI mouse lines were made at the transgenic core laboratory of Johns Hopkins University School of Medicine by using the CRISPR/Cas9 system. Suction-pipette recordings, analyses of light responses and dark noise, power spectral analysis, spectrophotometry, histology, and other experimental details are provided in *SI Appendix, Materials and Methods*.

Data, Materials, and Software Availability. All study data are included in the article and/or *SI Appendix*.

ACKNOWLEDGMENTS. We thank Jeremy Nathans at Johns Hopkins University School of Medicine for discussion during early stages of this work. We also thank all members of the Yau laboratory for discussions. This work was supported by NIH Grant EY006837 (to K.-W.Y.), the António Champalimaud Vision Award, Portugal (to K.-W.Y.), NS050274 (Multiphoton Imaging Core at Johns Hopkins University), the Daniel Nathans Scientific Innovator Award, Johns Hopkins University School of Medicine (K.-W.Y.), and the Beckman-Argyros Vision Award (K.-W.Y.) from the Arnold and Mabel Beckman Foundation.

Author affiliations: [a]Solomon H. Snyder Department of Neuroscience, Johns Hopkins University School of Medicine, Baltimore, MD 21205; [b]Biochemistry, Cellular and Molecular Biology Graduate Program, Department of Ophthalmology, Johns Hopkins University School of Medicine, Baltimore, MD 21205; [c]Department of Physiology and Neuroscience, Keck School of Medicine, University of Southern California, Los Angeles, CA 90033; and [d]Department of Molecular Biology and Genetics (Emeritus), Johns Hopkins University School of Medicine, Baltimore, MD 21205

1. H. F. Mendes, J. van der Spuy, J. P. Chapple, M. E. Cheetham, Mechanisms of cell death in rhodopsin retinitis pigmentosa: Implications for therapy. *Trends Mol. Med.* **11**, 177–185 (2005).
2. D. Athanasiou *et al.*, The molecular and cellular basis of rhodopsin retinitis pigmentosa reveals potential strategies for therapy. *Prog. Retin Eye Res.* **62**, 1–23 (2018).
3. C. Zeitz, A. G. Robson, I. Audo, Congenital stationary night blindness: An analysis and update of genotype-phenotype correlations and pathogenic mechanisms. *Prog. Retin Eye Res.* **45**, 58–110 (2015).
4. A. H. Kim *et al.*, Congenital stationary night blindness: Clinical and genetic features. *Int J. Mol. Sci.* **23**, 14965 (2022).

5. V. R. Rao, D. D. Oprian, Activating mutations of rhodopsin and other G protein-coupled receptors. *Annu. Rev. Biophys. Biomol. Struct.* **25**, 287–314 (1996).
6. S. D. McAlear, T. W. Kraft, A. K. Gross, 1 rhodopsin mutations in congenital night blindness. *Adv. Exp. Med. Biol.* **664**, 263–272 (2010).
7. P. S. Park, Constitutively active rhodopsin and retinal disease. *Adv. Pharmacol.* **70**, 1–36 (2014).
8. P. A. Sieving *et al.*, Dark-light: Model for nightblindness from the human rhodopsin Gly-90–>Asp mutation. *Proc. Natl. Acad. Sci. U.S.A.* **92**, 880–884 (1995).
9. P. A. Sieving *et al.*, Constitutive "light" adaptation in rods from G90D rhodopsin: A mechanism for human congenital nightblindness without rod cell loss. *J. Neurosci.* **21**, 5449–5460 (2001).
10. A. K. Gross, V. R. Rao, D. D. Oprian, Characterization of rhodopsin congenital night blindness mutant T94I. *Biochemistry* **42**, 2009–2015 (2003).
11. S. Jin, M. C. Cornwall, D. D. Oprian, Opsin activation as a cause of congenital night blindness. *Nat. Neurosci.* **6**, 731–735 (2003).
12. A. M. Dizhoor *et al.*, Night blindness and the mechanism of constitutive signaling of mutant G90D rhodopsin. *J. Neurosci.* **28**, 11662–11672 (2008).
13. P. R. Robinson, G. B. Cohen, E. A. Zhukovsky, D. D. Oprian, Constitutively active mutants of rhodopsin. *Neuron* **9**, 719–725 (1992).
14. V. R. Rao, G. B. Cohen, D. D. Oprian, Rhodopsin mutation G90D and a molecular mechanism for congenital night blindness. *Nature* **367**, 639–642 (1994).
15. S. Kawamura, A. T. Colozo, L. Ge, D. J. Müller, P. S. Park, Structural, energetic, and mechanical perturbations in rhodopsin mutant that causes congenital stationary night blindness. *J. Biol. Chem.* **287**, 21826–21835 (2012).
16. A. Singhal *et al.*, Insights into congenital stationary night blindness based on the structure of G90D rhodopsin. *EMBO Rep.* **14**, 520–526 (2013).
17. M. J. Brooks, H. K. Rajasimha, J. E. Roger, A. Swaroop, Next-generation sequencing facilitates quantitative analysis of wild-type and Nrl(-/-) retinal transcriptomes. *Mol. Vis.* **17**, 3034–3054 (2011).
18. P. D. Calvert *et al.*, Phototransduction in transgenic mice after targeted deletion of the rod transducin alpha -subunit. *Proc. Natl. Acad. Sci. U.S.A.* **97**, 13913–13918 (2000).
19. J. Xu *et al.*, Prolonged photoresponses in transgenic mouse rods lacking arrestin. *Nature* **389**, 505–509 (1997).
20. W. W. S. Yue *et al.*, Elementary response triggered by transducin in retinal rods. *Proc. Natl. Acad. Sci. U.S.A.* **116**, 5144–5153 (2019).
21. D. Silverman *et al.*, Dark noise and retinal degeneration from D190N-rhodopsin. *Proc. Natl. Acad. Sci. U.S.A.* **117**, 23033–23043 (2020).
22. A. Mendez *et al.*, Role of guanylate cyclase-activating proteins (GCAPs) in setting the flash sensitivity of rod photoreceptors. *Proc. Natl. Acad. Sci. U.S.A.* **98**, 9948–9953 (2001).
23. W. He, C. W. Cowan, T. G. Wensel, RGS9, a GTPase accelerator for phototransduction. *Neuron* **20**, 95–102 (1998).
24. C. K. Chen *et al.*, Slowed recovery of rod photoresponse in mice lacking the GTPase accelerating protein RGS9-1. *Nature* **403**, 557–560 (2000).
25. D. A. Baylor, G. Matthews, K. W. Yau, Two components of electrical dark noise in toad retinal rod outer segments. *J. Physiol.* **309**, 591–621 (1980).
26. K. Nakatani, T. Tamura, K. W. Yau, Light adaptation in retinal rods of the rabbit and two other nonprimate mammals. *J. Gen. Physiol.* **97**, 413–435 (1991).
27. B. Katz, R. Miledi, The statistical nature of the acetycholine potential and its molecular components. *J. Physiol.* **224**, 665–699 (1972).
28. V. Kefalov, Y. Fu, N. Marsh-Armstrong, K. W. Yau, Role of visual pigment properties in rod and cone phototransduction. *Nature* **425**, 526–531 (2003).
29. Y. Fu, V. Kefalov, D. G. Luo, T. Xue, K. W. Yau, Quantal noise from human red cone pigment. *Nat. Neurosci.* **11**, 565–571 (2008).
30. C. K. Chen *et al.*, Abnormal photoresponses and light-induced apoptosis in rods lacking rhodopsin kinase. *Proc. Natl. Acad. Sci. U.S.A.* **96**, 3718–3722 (1999).
31. J. Chen, M. I. Simon, M. T. Matthes, D. Yasumura, M. M. LaVail, Increased susceptibility to light damage in an arrestin knockout mouse model of Oguchi disease (stationary night blindness). *Invest. Ophthalmol. Vis. Sci.* **40**, 2978–2982 (1999).
32. J. M. Kim *et al.*, Structural origins of constitutive activation in rhodopsin: Role of the K296/E113 salt bridge. *Proc. Natl. Acad. Sci. U.S.A.* **101**, 12508–12513 (2004).
33. N. Kubatova *et al.*, Light dynamics of the retinal-disease-relevant G90D bovine Rhodopsin mutant. *Angew Chem. Int. Ed. Engl.* **59**, 15656–15664 (2020).
34. T. A. Zvyaga, K. Fahmy, F. Siebert, T. P. Sakmar, Characterization of the mutant visual pigment responsible for congenital night blindness: A biochemical and Fourier-transform infrared spectroscopy study. *Biochemistry* **35**, 7536–7545 (1996).
35. T. Wang, J. Chen, Induction of the unfolded protein response by constitutive G-protein signaling in rod photoreceptor cells. *J. Biol. Chem.* **289**, 29310–29321 (2014).
36. K. M. Nishiguchi *et al.*, Phenotypic features of Oguchi disease and Retinitis pigmentosa in patients with S-antigen mutations: A long-term follow-up study. *Ophthalmology* **126**, 1557–1566 (2019).